GDCh Research Article Angewandte International Edition Chemie www.angewandte.org

How to cite: *Angew. Chem. Int. Ed.* **2025**, *64*, e202517059
doi.org/10.1002/anie.202517059

Contact-Electro-Chemistry

# Sustainable Fluorinated Silicon Dielectric Design for Enhanced Contact-Electro-Chemistry

*Ting Gan[+], Zhijian Li[+], Shaoxin Li[+], Hanbin Liu,* Gehan Amaratunga,* Zhonglin Wang,* and Di Wei**

**Abstract:** Solid–liquid contact electrification (CE) has recently emerged as a powerful means of initiating interfacial chemical reactions via charge transfer. Fluorinated ethylene propylene (FEP) and polytetrafluoroethylene (PTFE) are frequently employed as solid dielectrics owing to their fluorine-rich surfaces, which exhibit strong electron-withdrawing characteristics. However, their high environmental cost and poor surface modifiability hinder the broader adoption of contact-electro-chemistry (CE-Chemistry). Here, we report a low-cost and tunable dielectric alternative based on silicon powder, surface-functionalized with fluorinated alkyl chains to mimic the interfacial properties of conventional fluoropolymers. Fluorinated silicon powders (F-Si) were synthesized via a mild self-assembly approach using 1H,1H,2H,2H-perfluorodecyltriethoxysilane. The resulting F-Si powders exhibited a 30-fold enhancement in methyl orange degradation efficiency compared to unmodified silicon, and a 4-fold improvement in phenol degradation relative to size-matched FEP powder. In contrast, aggressive fluorination via piranha-assisted pretreatment (P-F-Si) induced particle aggregation and loss of CE reactivity, highlighting the importance of controlled surface engineering. Furthermore, CE-Chemistry enabled the first noble-metal-free oxidation of $I^-$ to $I_3^-$, establishing a low-energy, cost-effective paradigm for catalytic iodine conversion. Together, these advances provide a sustainable materials design framework for CE-Chemistry, with broad implications for scalable, green chemical transformation technologies.

## Introduction

Interfaces offer a promising platform for initiating chemical reactions, particularly catalytic processes relevant to environmental remediation and energy conversion.[1–5] Conventional catalytic approaches, such as photocatalysis[6,7] and electrocatalysis,[8,9] rely on external stimuli, including light and applied voltage, and typically require specialized catalysts featuring narrow bandgaps or high densities of surface-active sites. In contrast, chemical reactions driven by contact electrification (CE) at solid–liquid interfaces have recently attracted increasing attention, owing to their ability to proceed without external light or voltage.[10–16] Moreover, CE induces interfacial electron transfer that establishes a stable surface electric field with strong capability for driving chemical reactions.[17] Enabled by interfacial charge transfer, CE between solids and liquids can generate reactive oxygen species (ROS) in situ, facilitating the catalytic degradation of organic pollutants,[18,19] a process termed contact-electro-catalysis (CEC).[3,12,20–22] More recently, the role of solid–liquid CE has expanded beyond catalysis to encompass redox reactions,[23,24] polymerization reactions,[23] fluorescence modulation,[25] and other chemical transformations in nonaquous system,[17,26,27] a broader framework referred to as contact-electro-chemistry (CE-Chemistry).[28]

[*] T. Gan[+], Z. Li[+], H. Liu
College of Bioresource Chemical and Materials Engineering, Shaanxi Provincial Key Laboratory of Papermaking Technology and Specialty Paper Development, Shaanxi University of Science & Technology, Xi'an 710021, P.R. China
E-mail: liuhanbin@sust.edu.cn

T. Gan[+], S. Li[+], Z. Wang, D. Wei
Beijing Institute of Nanoenergy and Nanosystems, Chinese Academy of Sciences, Beijing 101400, P.R. China
E-mail: zlwang@binn.cas.cn
weidi@binn.cas.cn

S. Li[+]
School of Nanoscience and Engineering, University of Chinese Academy of Sciences, Beijing 100049, P.R. China

G. Amaratunga
Zhejiang University–University of Illinois at Urbana Champagne Institute (ZJUI) and School of Information Science and Electronics, Zhejiang University International Campus, Haining, P.R. China
E-mail: gehan@intl.zju.edu.cn

G. Amaratunga
Electrical Engineering Division, Department of Engineering, University of Cambridge, Cambridge CB3 0FA, UK

G. Amaratunga
School of Critical Materials for Integrated Circuits, Shenzhen Polytechnic University, 7098 Liuxian Avenue, Shenzhen 518055, P.R. China

D. Wei
Centre for Photonic Devices and Sensors, University of Cambridge, 9 JJ Thomson Avenue, Cambridge CB3 0FA, UK

[+] These authors contributed equally to this work.

Additional supporting information can be found online in the Supporting Information section

In CE-Chemistry, fluorinated polymers such as polytetrafluoroethylene (PTFE) and fluorinated ethylene propylene (FEP) have emerged as the most widely used dielectric materials.[29,30] Their exceptional electronegativity, stemming from densely packed fluorine atoms, promotes strong interfacial charge transfer and the generation of a significantly enhanced interfacial electric field.[31,32] Such electric field has been effectively harnessed to drive a variety of reactions, including the green synthesis of hydrogen peroxide,[33,34] the degradation of organic pollutants,[18,35] and the recovery of precious metals from spent lithium-ion batteries.[3] Despite these advantages, fluoropolymers present several critical limitations that hinder their broader applicability. Their high recycling challenge and complex, requiring harsh conditions and specialized processing techniques.[36,37] Additionally, their low surface energy and chemical inertness impede further functionalization, restricting opportunities to tailor their electronic or structural properties for specific reaction environments.[38,39] These constraints, combined with their rigid molecular architecture and poor scalability, underscore the need for alternative dielectric materials that are cost-effective, environmentally benign, and structurally versatile, while maintaining or surpassing the interfacial charge transfer efficiency necessary for high-performance CE-Chemistry.

In this work, we present a functionalized dielectric material (F-Si) fabricated by grafting 1H, 1H, 2H, 2H-perfluorodecyltriethoxysilane (FDTES) onto silicon powder, a cost-effective, structurally versatile substrate. The optimized F-Si demonstrated a striking 30-fold increase in methyl orange (MO) degradation efficiency compared to pristine silicon powder, and a 4-fold enhancement in phenol degradation relative to FEP powder of similar particle size. To further regulate surface fluorine density, a hydroxylation pretreatment with piranha solution was introduced prior to fluorination, producing a high-fluorine variant denoted P-F-Si. Despite its elevated fluorine content, P-F-Si exhibited reduced catalytic performance due to particle aggregation, which diminished the accessible solid–liquid interfacial area and the number of active sites. These results highlight the pivotal role of fluorination strategy and particle morphology in dictating interfacial reactivity. Importantly, the mild fluorination approach employed here not only improved catalytic efficiency but also reduced fabrication costs and minimized fluorinated waste output. Through the synergistic modulation of resistivity and surface chemistry, F-Si offers a new design blueprint for constructing green, efficient, and scalable catalytic systems in CE-Chemistry.

## Results and Discussion

### Investigations on the Degradation of MO

CE-Chemistry emerges as an innovative paradigm in green chemistry, leveraging its metal-free catalytic nature and versatile material compatibility. Beyong the commonly employed fluorinated solid dielectric such as FEP and PTFE, this study introduce silicon as a dielectric material, capitalizing on its tunable surface functionalization potential for enhanced CE-Chemical reaction efficiency. As illustrated in Figure 1a, 10 mg of dielectric material was added to 10 mL of 5 ppm MO solution. Mechanical stirring was employed to enhance solid–liquid interfacial contact. The molecular structure of MO is shown in Figure S1. The as-prepared suspension was then ultrasonicated at 40 kHz with a power of 120 W, while the reaction temperature was controlled using a thermostatic circulator (Figure S2). Under identical experimental conditions, MO degradation was performed using two silicon powders with resistivities (10 and 100 Ω·m), respectively. As shown in Figure 1b, in the CE-Chemistry system, 10 Ω·m silicon powder exhibited a degradation rate of 50% after 1 h of ultrasonication treatment, whereas no significant degradation was observed for 100 Ω·m silicon powder under identical conditions. Upon extending the reaction duration to 4 h, the degradation rate of MO solution surged to 35% (100 Ω·m) and 87% (10 Ω·m), respectively, with a difference in reaction efficiency of 2.5 times. The enhanced catalytic efficiency may originates from the low-resistivity silicon powder (10 Ω·m) promoting the generation of a higher density of electrons. These electrons are readily captured by molecular oxygen, leading to the formation of a greater concentration of superoxide radicals ($^{\cdot}O_2^-$). The formation of these dielectric material induced ROS significantly improves the degradation efficiency of the pollutants.[31]

To overcome the inherent activity limitations of silicon materials, FDTES was used to perform surface grafting fluorination on silicon powder. The resulting material (denoted as F-Si) enhances the surface electron affinity through C─F bonds. As depicted in Figure S3, the time-dependent UV–vis spectra of MO degradation mediated by F-Si in the CE-Chemistry system indicated 50% degradation efficiency after 5 min sonication treatment. Figure S4 shows the color change of the MO solution under different ultrasonic treatment times. When the ultrasonic treatment lasted for about 40 min, the solution turned transparent. The degradation efficiency of F-Si is approximately 29 times higher than that of unfluorinated silicon powder (Figure 1c). To further regulate the density of fluorine atom density on the silicon surface, piranha solution was used to pre-hydroxylate the silicon powder, followed by FDTES for fluorination treatment, yielding a high fluorine density material denoted as P-F-Si. The degradation efficiency of MO by P-F-Si are shown in Figure S5. F-Si exhibits superior degradation efficiency compared to both P-F-Si and Si. This phenomenon may be attributed to the piranha treatment induced increase in hydroxyl group density on the silicon surface, which promotes particle aggregation and reduces the specific surface area, thereby diminishing the reaction efficiency. The consistent trends in MO degradation efficiency (Figure S5) and charge transfer (Figure S6) among F-Si, P-F-Si and Si establish a clear correlation between CE performance and chemical reactivity. To further clarify this mechanism, the pH value changes of the aqueous solutions were monitored after ultrasonication treatment in the presence of F-Si and P-F-Si, respectively. As shown in Figure S7, the pH of deionized (DI) water remained neutral, whereas both F-Si and P-F-Si systems exhibited a pH decrease under identical ultrasonic treatment conditions. Notably, the pH reduction was more pronounced in the F-Si aqueous

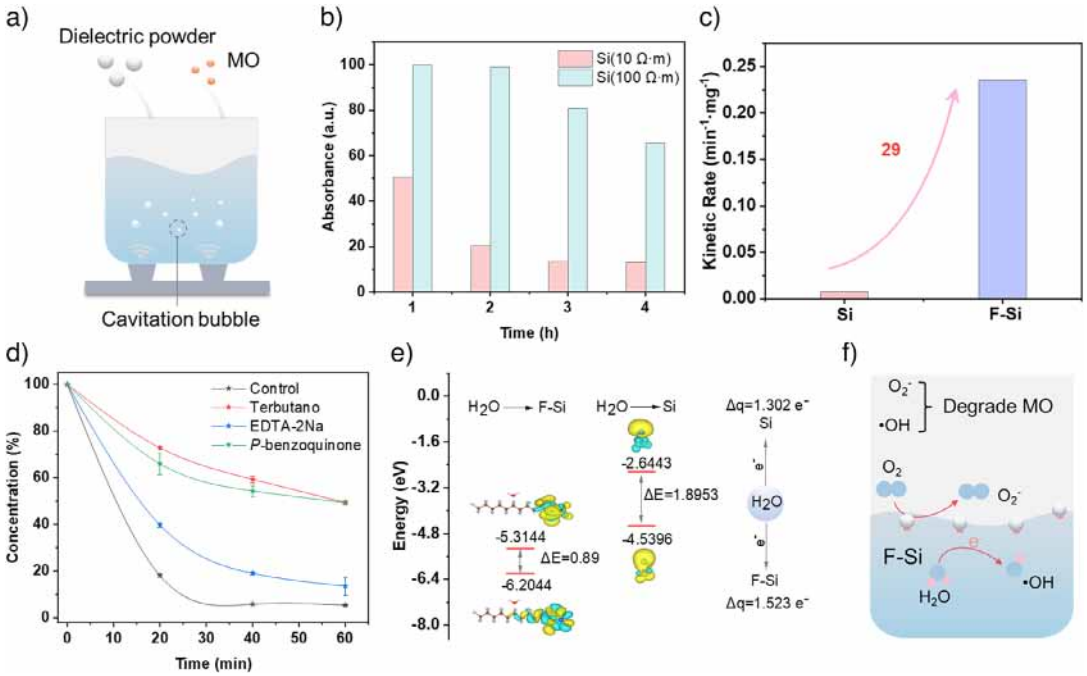


***Figure 1.*** Degradation of MO by CE-Chemistry. a) Graphical description of the experimental set-up. b) Degradation of MO with different resistivities silicon powder. c) Comparison of the degradation efficiency of MO by Si and F-Si. d) Evolution of MO concentration in conditions of various radical scavengers. Ter-butanol, *p*-benzoquinone, and EDTA-2Na are regarded as ·OH, $^{\cdot}O_2^-$, and proton scavengers, respectively. e) DFT simulations of electron transfer energy barriers and electron transfer quantities in different dielectric materials. f) The mechanism of MO degradation by radicals generated through CE-Chemistry. Error bars represent standard deviations for three reproduced experiments.

solution. This phenomenon may be attributed to the CE effect, wherein water molecules transfer electrons to dielectric materials and generate hydrogen ions ($H^+$). These results demonstrate that F-Si, as a novel dielectric material, exhibits superior electron transfer efficiency at solid–liquid interfaces, thereby significantly enhancing CE-Chemistry activity. Given the potential influence of temperature on chemical reactions, we systematically investigated MO degradation efficiency at different temperatures. Unexpectedly, the degradation efficiency decreased with increasing temperature (Figure S8), contrary to the conventional expectation from the Arrhenius equation.[40] This anomalous behavior reflects the interfacial nature of CE-Chemistry: higher temperatures enhance ionic mobility, which accelerates electrical double layer (EDL) formation and intensifies screening effects that suppress interfacial electron transfer.[17] To ensure optimal reaction efficiency, the reaction temperature was therefore maintained at 20 °C using a thermostated circulating water bath.

To systematically evaluate the CE-Chemical performance of F-Si, phenol was selected as a model organic pollutant for degradation, with FEP powder serving as the control material. As illustrated in Figure S9, in the CE-Chemistry system, the degradation efficiency of phenol by F-Si consistently surpassed that of FEP. After 4 h of ultrasonication treatment, the phenol degradation efficiency of F-Si was four times higher than that of FEP powder with the same particle size. To elucidate the degradation mechanism, ·OH concentrations induced by different dielectric materials in CE-Chemistry were quantitatively analyzed via UV–vis spectroscopy (Figure S10). The results demonstrated that ·OH generation with F-Si consistently exceeded that with FEP. This phenomenon might be attributed to the superior CE capability of F-Si. Furthermore, pH monitoring of the aqueous solution during ultrasonication revealed that the pH of the F-Si system was consistently lower than that of FEP, stabilizing at approximately 3.0 after 5 h (Figure S11). This integrated evidence confirms that enhancing the CE process significantly boosts catalytic efficiency in the reaction. This study not only validates that resistivity modulation and surface fluorination engineering are effective strategies for optimizing catalytic reactions, but also provides a new paradigm for designing high-performance, recyclable green catalytic materials.

Radical quenching experiments were employed to illustrate the contribution mechanism of ROS during the degradation process of MO. In this study, ter-butanol, *p*-benzoquinone and ethylenediaminetetraacetic acid disodium salt (EDTA-2Na) are regarded as ·OH, $^{\cdot}O_2^-$, and holes ($h^+$) scavengers, respectively. The degradation efficiency of MO was observed at different time intervals.[35] As shown in Figure 1d, the degradation efficiency of MO was significantly suppressed in the presence of tert–butanol and *p*–benzoquinone, confirming that both ·OH and $^{\cdot}O_2^-$ dominated the degradation process. The relationship between the concentration of dissolved $O_2$ and the degradation rate was further explored under different atmospheric conditions (air, oxygen, and argon). The fastest degradation rate (94.28%) was achieved in air, whereas the lowest (87.02%) was observed under an argon atmosphere (Figure S12). Notably, the degradation rate decreased to 90.82% when pure oxygen was introduced, which may be

attributed to the inhibition of electron induction and transfer during CE under a strongly oxidizing atmosphere, thereby reducing the catalytic activity.[41] The superior catalytic activity of F-Si can be directly correlated with its structural and electronic features. Density functional theory (DFT) calculations (Figure 1e) reveal that F-Si possesses the lower energy barrier for electron transfer and the higher theoretical charge transfer capacity than Si. Therefore, surface fluorination of F-Si should play a decisive role in enhancing CE performance by increasing surface electronegativity, stabilizing interfacial charges, and improving hydrophobicity. The degradation mechanism of MO is depicted in Figure 1f. Fluorine atoms in F-Si, acting as strong electron-withdrawing groups, which enhance the efficiency of electron transfer at the solid–liquid interface during CE process. Specifically, ultrasonic cavitation facilitates continuous contact-separation cycles between solid and liquid. This drives interfacial charge transfer during CE process, generating ROS that ultimately degrade MO efficiently.

### *Characterization of the Dielectric Powders*

The structural diagram of silicon surface after fluorination treatment is shown in Figure 2a. Silicon powder with a native $SiO_2$ layer was first immersed in a mixed solution of FDTES and isooctane to enable self-assembly, yielding fluorinated silicon (F-Si). To increase the surface grafting density of fluorine atoms, a hydrophilic pretreatment was applied. The silicon powder was treated with piranha solution ($H_2SO_4$:$H_2O_2$ = 7:3) at room temperature to enhance surface hydroxylation, followed by FDTES self-assembly in isooctane. This process yielded the piranha-treated, fluorinated silicon powder, denoted as P-F-Si. The chemical composition of the modified silicon surface was detected by X-ray photoelectron spectroscopy (XPS). The obvious F1s peak of F-Si and P-F-Si were observed at 687 eV, attributed to covalent C─F bonds in FDTES chains (Figure 2b). Furthermore, the F1s peak intensity of P-F-Si pretreated with piranha solution was significantly higher than that of F-Si, indicating that piranha pretreatment enhanced the surface hydroxyl density, promoting the covalent grafting of more FDTES chains, thereby increasing the surface density of fluorine atoms. The absence of peaks at 684 eV (characteristic of inorganic fluorides) further verifies the absence of physical adsorption, demonstrating the successful fluorine modification of FDTES on the silicon surface. The corresponding Si2p, O1s, C1s and F1s XPS spectra of Si, F-Si and P-F-Si were displayed in Figures S13–S15, respectively.

Notably, the observation of Si─O bonds in Si powder confirms the existence of a surface silicon oxide layer. The oxide layer facilitates subsequent fluorinated grafting by providing reactive surface sites. The presence of a surface silicon oxide layer was further confirmed by Fourier transform infrared (FTIR) spectroscopy (Figure S16), showing characteristics absorption at 800, 1095, and 1261 $cm^{-1}$ (corresponding to S─O─Si bond) and 960 $cm^{-1}$ (corresponding to Si─OH bond). FTIR spectroscopy of F-Si and P-F-Si surfaces confirmed the presence of fluorocarbon functional groups, evidenced by strong absorption peaks at 1216 $cm^{-1}$ (attributed to C─F stretching vibrations in ─CF, $─CF_2$ and $─CF_3$ groups) and additional absorption peaks at 576, 754, and 1122 $cm^{-1}$ (corresponding to the vibration of C─F bond in ─CF, $─CF_2$ and $─CF_3$ groups). The self-assembled surface was energy-dispersive X-ray spectroscopy (EDS) analysis also confirmed the above results (Figure 2c). X-ray diffraction (XRD) analysis (Figure S17) confirms the retention of Si's crystalline structure after fluorination, as evidenced by invariant characteristic diffraction peaks at 28.4°, 47.3°, 56.1°, 69.1° and 76.4° (corresponding to (111), (220), (311), (400) and (331) planes, respectively).

To quantitatively evaluate the effect of fluorination modification on the wettability of silicon powder surface, the contact angles of the silicon powder before and after modification were measure and compared (Figure 2d). The contact angle of the silicon powder before modification was 13.78°, while the contact angle of F-Si and P-F-Si after modification increased to 125.27° and 129.6°, indicating significantly enhanced hydrophobicity of the silicon surface after fluorination treatment. The dispersion behavior of Si, F-Si, and P-F-Si in MO solution further confirms the success of fluorination modification. It is worth noting that the interfacial contact state between particles and water is governed not only by the static contact angle, but also by particle size, morphology, dispersion, and wetting state. As shown in the dispersion states of F-Si and P-F-Si in MO solution (Figure 2d), both materials are hydrophobic, yet their distinct aggregation behaviors alter buoyancy and interfacial wetting. P-F-Si aggregates more readily, promoting local wetting and gravitational settling, whereas F-Si remains more dispersed, thereby sustaining a stable air layer and stronger apparent hydrophobicity. Smaller particles have also been reported to form more uniform climbing films on vessel walls.[42] In agreement, the larger P-F-Si particles are more prone to aggregation and sedimentation (Figure 2d), appearing less hydrophobic at the water surface than F-Si. The particle size analysis in Figure 2e demonstrates that the particle size of all fluorinated silicon powders increased, with the P-F-Si sample exhibiting a more significant increase. This result was further confirmed by the scanning electron microscope (SEM) images provided in Figure S18. This phenomenon may be attributed to the introduction of abundant hydroxyl groups on the silicon powder surface following piranha solution treatment, where hydrogen bonding interactions intensify interparticle agglomeration. The Brunauer–Emmett–Teller (BET) specific surface areas test further confirmed (Figure 2f) that P-F-Si has the lowest specific surface area, which may led to a decrease in solid–liquid CE efficiency and diminish the degradation of MO. Figure S19 shows the nitrogen adsorption–desorption isotherm of Si, F-Si, and P-F-Si.

To detect the generation of radicals in the CE-Chemistry system, 1,2-diaminobenzene (OPD) served as a detection probe for ·OH.[1,43] The detection mechanism involves the oxidation of OPD by ·OH to form diaminophenothiazine (DAP), which exhibits a characteristic absorption peak at 424 nm (Figure 3a). As shown in Figure 3b, which depicts the ·OH concentration distribution for different dielectric materials over time. The F-Si system exhibits significantly

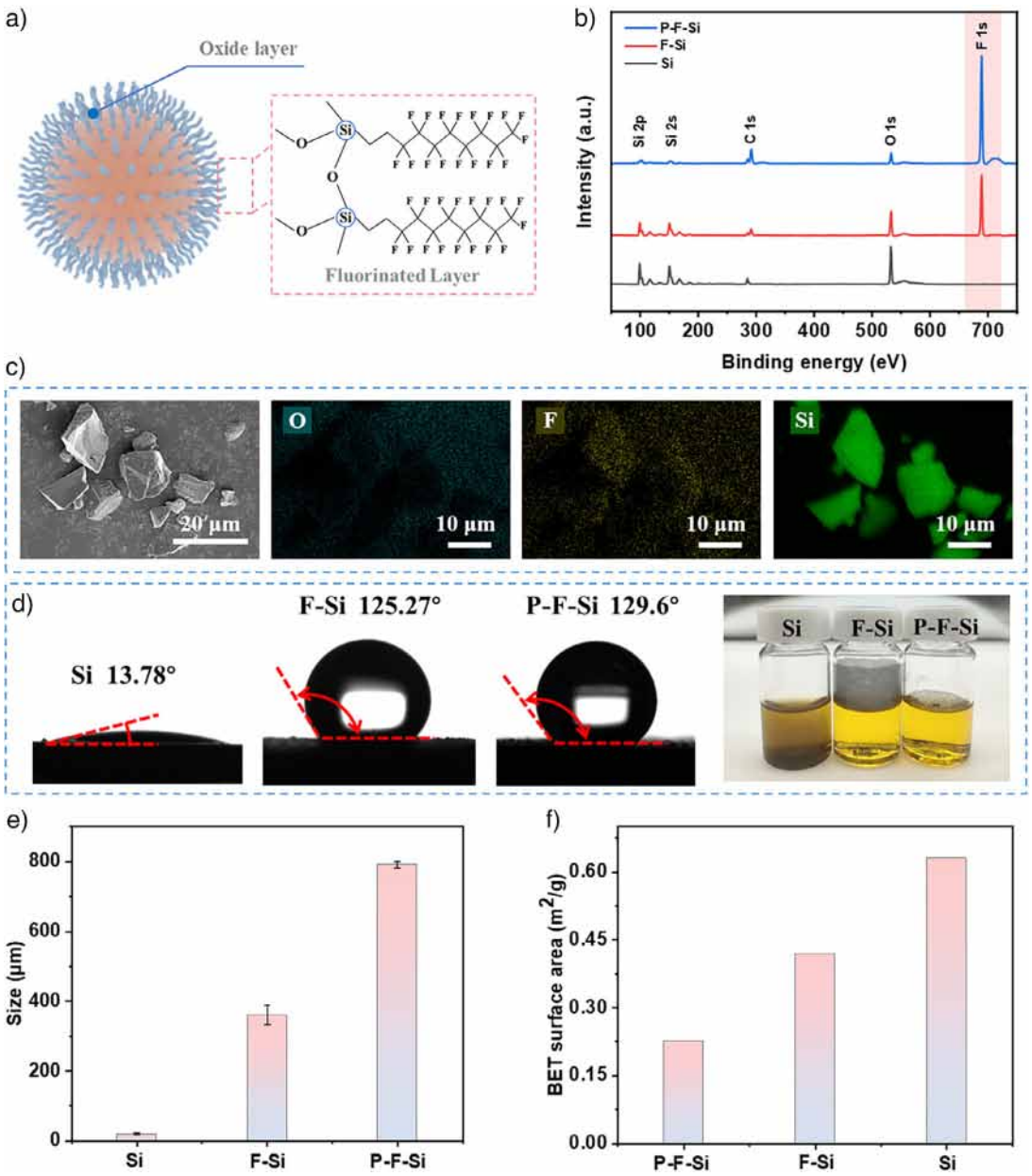


***Figure 2.*** The design and characterization of silicon powder fluorination. a) Schematic diagram of self-assembled FDTES monolayer formed on the silicon powder surface. b) XPS spectra of the Si, F-Si, and P-F-Si surface, the latter showing intense F1s peak. c) EDS images of F-Si. d) Contact angles of Si, F-Si, and P-F-Si, and optical photographs of their dispersion states in MO solution. e) The size distribution and f) BET specific surface areas of Si, F-Si, and P-F-Si. Error bars represent standard deviations for three reproduced experiments.

higher ·OH production than the other two dielectric materials. This results are related to the efficiency of CE at solid–liquid interface in CE-Chemistry systems. Electron paramagnetic resonance (EPR) spectroscopy was conducted to measure and compare the electron transfer under different dielectric materials. 5,5-dimethyl-1-pyrroline *N*- oxide (DMPO) is the capture for ·OH, the specific reaction mechanism is shown in Figure 3a. In Figure 3c, we observe the signal produced by the adducts obtained from the reaction between DMPO and ·OH, namely DMPO-·OH, after 30 min of ultrasonication in presence of these three materials. The highest intensity of the ·OH, is exhibited with F-Si, followed by P-F-Si and Si. The comparison among P-F-Si, F-Si, and Si provides insight into their overall performance in CE-driven chemistry. Effective CE reactivity is not dictated by particle size alone, but by the combined influence of surface functionalization, dispersion, and aggregation. Although the larger size of P-F-Si reduces particle number per unit mass, surface fluorination enhances its CE ability, resulting in stronger reactivity than unmodified Si (Figure 3b,c). However, its stronger aggregation diminishes CE performance relative to F-Si, which possesses the same fluorination but maintains better dispersion. Faraday cup measurements further confirm this trend: P-F-Si carries more charge than Si but less than F-Si (Figure S6), suggesting

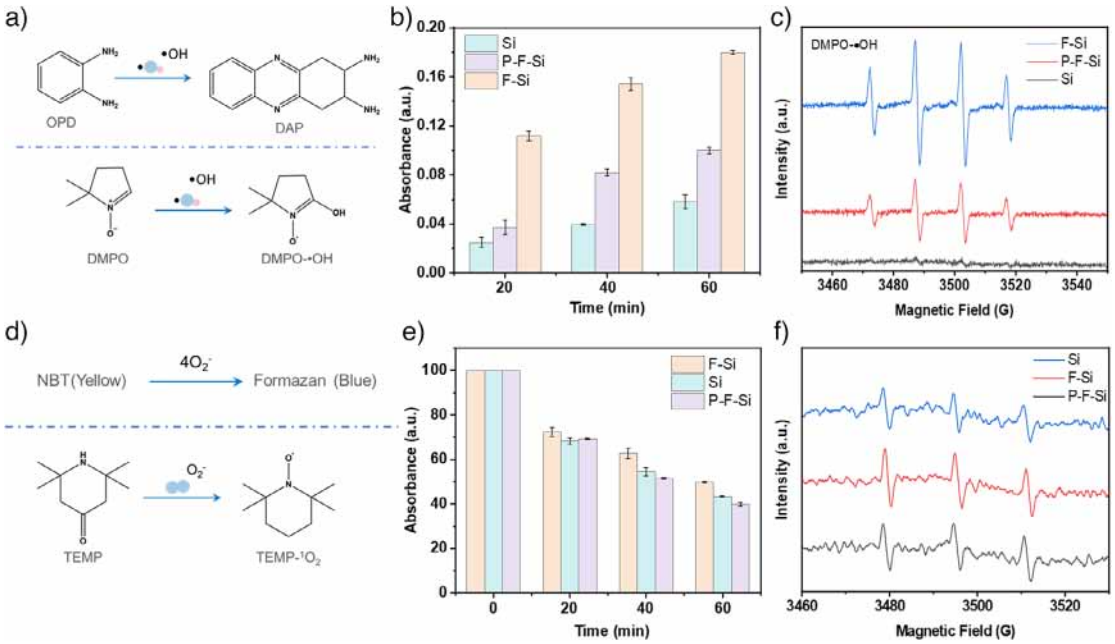


***Figure 3.*** Investigation on the contribution of radicals to degradation of MO. a) The generation of ·OH in the CE-Chemistry system was detected from the top to the bottom by UV–vis and EPR. b) Evolution of OPD solution absorbance treated with different three dielectric materials (Si, F-Si, P-F-Si). c) EPR spectra of DMPO-·OH were recorded after ultrasonication treatment in the presence of the dielectric material. d) The generation of $^{\cdot}O_2^-$ in the CE-Chemistry system was detected from the top to the bottom by UV–vis and EPR. e) Evolution of NBT solution absorbance treated with different three dielectric materials (Si, F-Si, P-F-Si). f) EPR spectra of TEMP-$^1O_2$ were recorded after ultrasonication treatment in the presence of the dielectric material. Error bars represent standard deviations for three reproduced experiments.

a limited surface electrostatic electric field. These results highlight that distinct material characteristics, surface chemistry, morphology, and aggregation, collectively determine CE performance, interfacial electric fields, and subsequent chemical reactivity. On the other hand, $^{\cdot}O_2^-$ detection was performed using nitroblue tetrazolium (NBT) colorimetric assay.[3] The detection mechanism is shown in Figure 3d, yellow NBT changes to blue Formazan to indicate the presence of $^{\cdot}O_2^-$. Kinetic analysis indicated that there was no significant difference in the generation rate of $^{\cdot}O_2^-$ among the three dielectric materials (Figure 3e), which was consistent with the EPR results (Figure 3f): singlet oxygen ($^1O_2$), the oxidative product of $^{\cdot}O_2^-$,[44] was captured by 2,2,6,6-tetramethylpiperidine (TEMP).[31] The degradation process of MO is driven by the synergy of ·OH and $^{\cdot}O_2^-$, with ·OH playing a dominant role. F-Si significantly enhances the electron transfer efficiency at the solid–liquid interface due to its surface fluorination engineering, thereby increasing the CE-Chemistry activity.

Although particle aggregation is observed for P-F-Si, it is not inherently detrimental. On the contrary, it offers a valuable opportunity to compare systems with different effective interfacial areas and dispersion states, thereby advancing our understanding of how morphology and interfacial structure govern CE performance and chemical reactivity. There is an alternative hydroxylation strategy using oxygen plasma treatment (100 W, 10 min) as a dry, solvent-free, and mild pretreatment, followed by FDTES fluorination. XPS analysis (Figures S20 and S21) confirmed successful fluorine grafting, with a surface fluorine density comparable to that of F-Si (Table S1). As shown in Figure S22, the particle size of the plasma-assisted fluorinated material (Plasma-F-Si) is ~ 417 μm, substantially smaller than that of P-F-Si (~ 800 μm) but still lagger than that of F-Si (~ 360 μm). This improved particle dispersion, together with stable fluorination, accouters for the high catalytic activity of Plasma-F-Si, which was significantly higher than P-F-Si but slightly lower than F-Si in MO degradation experiments (Figure S23).

Finally, the cycling stability of F-Si as a dielectric material in the CE-Chemistry system was evaluated. After five consecutive cycles, F-Si showed negligible change in MO degradation performance (Figure S24). XPS spectra of the recycled F-Si powder (C1s, F1s, Si2p, and O1s) revealed no binding energy shifts or new peak formation (Figure S25), confirming that the surface chemical composition remained stable before and after reaction. Moreover, total organic carbon (TOC) analysis of the reaction system showed negligible variation in organic carbon concentration (Figure S26), further indicating the absence of carbon leaching or structural decomposition during the CE-Chemistry process. Together, these results validate the high chemical and structural stability of F-Si under the tested conditions. Overall, reactivity of CE-Chemistry is governed by the interplay of material resistivity, surface chemistry, and particle morphology. Low resistivity in dielectrics is beneficial as it promotes charge transport to the solid–liquid interface while retaining the dielectric character necessary for CE. Surface fluorination further enhances electronegativity, charge stability, and interfacial field strength, whereas smaller or well-dispersed particles increase effective interfacial area.

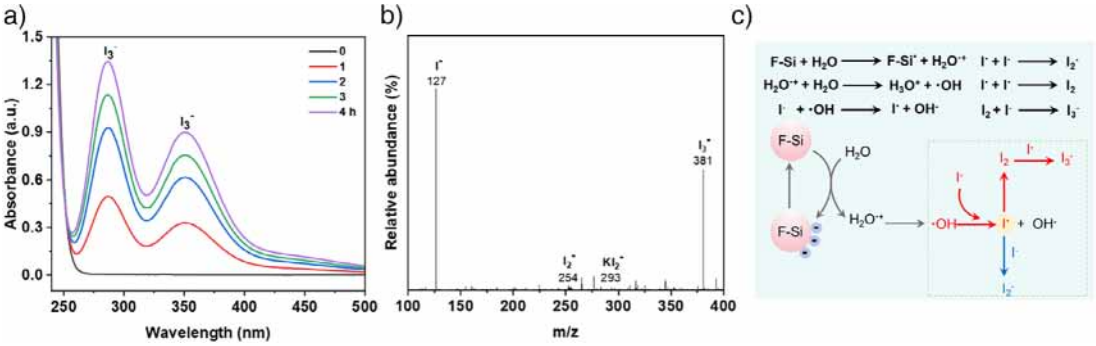


***Figure 4.*** $I^-$ oxidation to $I_3^-$ through CE-Chemistry. a) UV–vis spectra of a 10 mL aqueous NaI solution under different ultrasonication treatment times in the presence of F-Si powder. b) Typical mass spectrum showing the oxidation products of $I^-$. c) Proposed mechanism for the oxidation of $I^-$ by CE-Chemistry generated radicals.

### *Versatile Applications of CE-Chemistry*

Iodine active species, such as atomic iodine (I•), molecular iodine ($I_2$), and triiodide ($I_3^-$), play multifaceted roles in atmospheric chemistry and environmental catalysis.[45–49] For example, I• and $I_2$ catalyze ozone decomposition and oxidize gaseous elemental mercury ($Hg^0$) to $Hg^{2+}$ compounds, profoundly impacting atmospheric oxidative capacity and pollutant transport pathways.[50–52] In energy materials, $I_3^-$ as an efficient redox mediators can enhance the energy efficiency of zinc-air batteries.[53] Traditional generation of I• typically relies on thermal decomposition, photolysis, or chemical initiators, but these methods suffer from high energy demands, poor selectivity, and undesired side reactions, limiting practical utility. Here, we report for the first time that $I^-$ can be oxidized to $I_3^-$ via CE-Chemistry, enabling noble-metal-free iodine activation under mild conditions. This advance establishes a low-energy pathway for catalytic iodine conversion, with broad implications for atmospheric pollutant mitigation, green energy systems, and sustainable iodine cycling.

The oxidation reaction was achieved in 1 mM aqueous potassium iodide (KI) solution in presence of 10 mg of F-Si powder. To investigate the oxidation of KI process, aliquots were sampled at specific intervals and analyzed by UV–vis absorption spectroscopy. As shown in Figure 4a, the characteristic absorbance peak of $I_3^-$ at ~288 and ~352 nm was observed, the peak of $I_3^-$ increased as the ultrasonication time increased. This resulted was consistent with reported literature.[54–56] Figure 4b shows the mass spectrum of the KI solution after ultrasonic treatment for 4 h. A characteristic peak of the $I^-$ is observed at *m/z* 127, while the signal at *m/z* 293 is attributed to the $KI_2^-$. Additionally, the signal at *m/z* 254 corresponds to the $I_2^-$, formed via the combination of I• with $I^-$. The signal at *m/z* 381 is assigned to the $I_3^-$, generated by the binding of two I• to one $I^-$. The presence of $I_2^-$ and $I_3^-$ confirms the oxidative polymerization reaction of $I^-$ induced by the CE-Chemistry. Figure 4c summarizes and illustrates the proposed CE-Chemistry-driven oxidation mechanism of $I^-$. Firstly, $H_2O$ underwent continuous electron transfer toward the F-Si during the CE process in the formation of water radical cations. These water radical cations combine with water form hydronium cations and ·OH. The highly oxidative ·OH can oxidize $I^-$ to I•, where I• further evolves into the products $I_2^-$ and $I_3^-$ with other $I^-$ or I•. Therefore, the F-Si dielectric materials constructed via surface fluorination engineering strategy not only provide a straightforward approach to enhance the catalytic efficiency of CE-Chemistry, but also offer a highly promising solution for designing high-efficiency catalytic systems in chemical engineering and environmental energy fields.

## *Conclusion*

This study establishes that the reactivity of CE-Chemistry is governed by the resistivity, surface fluorination strategy, and particle size of the dielectric substrate. Low-resistivity silicon powder accelerates interfacial electron transfer, thereby enhancing catalytic activity. Through tailored surface fluorination, F-Si materials exhibit significantly boosted CE performance, achieving a 30-fold increase in MO degradation and a 4-fold improvement in phenol degradation compared to unmodified silicon and similarly sized FEP, respectively. While aggressive fluorination via piranha-assisted treatment increases fluorine grafting density, it also induces severe aggregation, diminishing surface area, and reactivity. In contrast, the mild self-assembly fluorination strategy not only preserves dispersity and surface accessibility but also offers a cost-effective and environmentally benign route for dielectric modification. Importantly, we demonstrate for the first time that CE-Chemistry can drive the oxidation of $I^-$ to $I_3^-$ without noble metal catalysts, substantially lowering energy input and material costs. This advance redefines the catalytic landscape of CE-Chemistry, with transformative implications for green energy technologies, atmospheric pollutant regulation, and sustainable iodine cycling, etc.

## *Author Contributions*

D. Wei and Z. L. Wang proposed the idea, H. B. Liu, Z. J. Li and G. Amaratunga participated the project. D. Wei and

S. X. Li guided the experimental test. T. Gan carried out the experiments. T. Gan, S. X. Li and D. Wei analyzed the corresponding data. T. Gan, S. X. Li and D. Wei wrote and revised the manuscript. All the authors discussed the results and commented on the manuscript.

## Acknowledgements

This work was supported by the National Natural Science Foundation (22479016), the National Natural Science Foundation of China (22078186), the Key Research and Development Project of Shaanxi Province (2024GX-YBXM-031, 2021GY-305), and the Natural Science Foundation of Shaanxi Provincial Department of Education (23JY014).

## Conflict of Interests

The authors declare no conflict of interest.

## Data Availability Statement

The data that support the findings of this study are available in the Supporting Information of this article.

**Keywords:** CE-Chemistry · Contact electrification · Interfacial charge transfer · Reactive oxygen species · Ultrasonication

[1] Y. Hu, W. Yang, Y. Ma, Y. Qiu, W. Wei, B. Wu, K. Li, Y. Li, Q. Zhang, R. Xiao, C. Hou, H. Wang, *Nat. Commun.* **2025**, *16*, 1692.
[2] R. Kusaka, S. Nihonyanagi, T. Tahara, *Nat. Chem.* **2021**, *13*, 306–311.
[3] H. Li, A. Berbille, X. Zhao, Z. Wang, W. Tang, Z. L. Wang, *Nat. Energy* **2023**, *8*, 1137–1144.
[4] B. Zhang, W. Xu, L. Peng, Y. Li, W. Zhang, Z. Wang, *Nature Reviews Electrical Engineering* **2024**, *1*, 218–233.
[5] N. Wang, Y. Liu, Y. Feng, J. Yang, Y. Wu, B. Zhang, Y. Li, B. Li, S. Wang, E. Ye, Y.-W. Zhang, X. J. Loh, F. Zhou, Z. Li, D. Wang, *Adv. Mater.* **2024**, *36*, 2303389.
[6] H. Hou, X. Zeng, X. Zhang, *Angew. Chem. Int. Ed.* **2020**, *59*, 17356–17376.
[7] Y. Ding, S. Maitra, S. Halder, C. Wang, R. Zheng, T. Barakat, S. Roy, L.-H. Chen, B.-L. Su, *Matter* **2022**, *5*, 2119–2167.
[8] L. Fan, X. Bai, C. Xia, X. Zhang, X. Zhao, Y. Xia, Z.-Y. Wu, Y. Lu, Y. Liu, H. Wang, *Nat. Commun.* **2022**, *13*, 2668.
[9] X. Hu, Z. Sun, G. Mei, X. Zhao, B. Y. Xia, B. You, *Adv. Energy Mater.* **2022**, *12*, 2201466.
[10] M. A. Mohajer, P. Basuri, A. Evdokimov, G. David, D. Zindel, E. Miliordos, R. Signorell, *Science* **2025**, *388*, 1426–1430.
[11] Y. Meng, Y. Xia, J. Xu, R. N. Zare, *Sci.Adv*. **2025**, *11*, eadt8979.
[12] N. Wang, W. Jiang, J. Yang, H. Feng, Y. Zheng, S. Wang, B. Li, J. Z. X. Heng, W. C. Ong, H. R. Tan, Y.-W. Zhang, D. Wang, E. Ye, Z. Li, *Nat. Commun.* **2024**, *15*, 5913.
[13] A. C. Aragonès, N. L. Haworth, N. Darwish, S. Ciampi, E. J. Mannix, G. G. Wallace, I. Diez-Perez, M. L. Coote, *Nature* **2016**, *531*, 88–91.
[14] J. Dong, J. Chen, W. Wang, Z. Wei, Z.-Q. Tian, F. R. Fan, *J. Am. Chem. Soc.* **2024**, *146*, 2227–2236.
[15] D. Zhang, X. Yuan, C. Gong, X. Zhang, *J. Am. Chem. Soc.* **2022**, *144*, 16184–16190.
[16] N. Wang, W. Jiang, H. Feng, J. Yang, B. Li, T. Yu, C. Du, J. Wang, J. Z. X. Heng, J. H. Pan, Y.-W. Zhang, D. Wang, E. Ye, Z. Li, *Small* **2025**, *21*, 2411815.
[17] J. Liu, Z. Yang, S. Li, Y. Du, Z. Zhang, J. Shao, M. Willatzen, Z. L. Wang, D. Wei, *J. Am. Chem. Soc.* **2024**, *146*, 31574–31584.
[18] Z. Wang, A. Berbille, Y. Feng, S. Li, L. Zhu, W. Tang, Z. L. Wang, *Nat. Commun.* **2022**, *13*, 130.
[19] Z. Wang, X. Dong, X.-F. Li, Y. Feng, S. Li, W. Tang, Z. L. Wang, *Nat. Commun.* **2024**, *15*, 757.
[20] Z. Wang, X. Dong, W. Tang, Z. L. Wang, *Chem. Soc. Rev.* **2024**, *53*, 4349–4373.
[21] Y. Su, A. Berbille, X.-F. Li, J. Zhang, M. PourhosseiniAsl, H. Li, Z. Liu, S. Li, J. Liu, L. Zhu, Z. L. Wang, *Nat. Commun.* **2024**, *15*, 4196.
[22] W. Li, J. Sun, M. Wang, J. Xu, Y. Wang, L. Yang, R. Yan, H. He, S. Wang, W.-Q. Deng, Z.-Q. Tian, F. R. Fan, *Angew. Chem. Int. Ed.* **2024**, *63*, e202403114.
[23] S. Li, Z. Zhang, P. Peng, X. Li, Z. L. Wang, D. Wei, *Nano Energy* **2024**, *122*, 109286.
[24] N. Wang, H. Feng, J. Yang, J. Zheng, Y. W. Zhang, N. Hadjichristidis, Z. Li, *Angew. Chem.* **2025**, *137*, e202500222.
[25] C. Xu, S. Li, Y. Zhang, Z. Wang, Z. L. Wang, D. Wei, *Nano Energy* **2025**, *134*, 110526.
[26] T. Gan, Z. Yang, S. Li, H. Qian, Z. Li, J. Liu, P. Peng, J. Bai, H. Liu, Z. Wang, D. Wei, *J. Am. Chem. Soc.* **2025**, *147*, 25407–25416.
[27] D. Wei, T. Lindfors, C. Kvarnström, L. Kronberg, R. Sjöholm, A. Ivaska, *J. Electroanal. Chem.* **2005**, *575*, 19–26.
[28] S. Li, J. Liu, Z. L. Wang, D. Wei, *Green Energy & Environment* **2025**, *10*, 937–966
[29] S. Li, J. Nie, Y. Shi, X. Tao, F. Wang, J. Tian, S. Lin, X. Chen, Z. L. Wang, *Adv. Mater.* **2020**, *32*, 2001307.
[30] H. Zou, Y. Zhang, L. Guo, P. Wang, X. He, G. Dai, H. Zheng, C. Chen, A. C. Wang, C. Xu, Z. L. Wang, *Nat. Commun.* **2019**, *10*, 1427.
[31] X. Dong, Z. Wang, Y. Hou, Y. Feng, A. Berbille, H. Li, Z. L. Wang, W. Tang, *J. Am. Chem. Soc.* **2024**, *146*, 28110–28118.
[32] C. Ye, D. Liu, Y. Gao, F. Liu, H. Xu, T. Jiang, Z. L. Wang, *Matter* **2025**, *8*, 102007.
[33] J. Zhao, X. Zhang, J. Xu, W. Tang, Z. Lin Wang, F. Ru Fan, *Angew. Chem. Int. Ed.* **2023**, *62*, e202300604.
[34] A. Berbille, X.-F. Li, Y. Su, S. Li, X. Zhao, L. Zhu, Z. L. Wang, *Adv. Mater.* **2023**, *35*, 2304387.
[35] W. Li, J. Tu, J. Sun, Y. Zhang, J. Fang, M. Wang, X. Liu, Z.-Q. Tian, F. Ru Fan, *Angew. Chem. Int. Ed.* **2025**, *64*, e202413246.
[36] J. Gardiner, *Aust. J. Chem.* **2015**, *68*, 13–22.
[37] J. Lv, Y. Cheng, *Chem. Soc. Rev.* **2021**, *50*, 5435–5467.
[38] H.-X. Sun, L. Zhang, H. Chai, H.-L. Chen, *Desalination* **2006**, *192*, 271–279.
[39] S.-J. Zhang, Y.-Y. Liu, S.-S. Lv, J.-P. Cheng, B. Liao, P. Pang, Z. Deng, L. He, *Nuclear Science and Techniques* **2022**, *33*, 90.
[40] K. J. Laidler, *J. Chem. Educ.* **1984**, *61*, 494.
[41] L. L. Sun, S. Q. Lin, W. Tang, X. Chen, Z. L. Wang, *ACS Nano* **2020**, *14*, 17354–17364.
[42] Y. Lai, H. Zhou, Z. Zhang, Y. Tang, J. W. C. Ho, J. Huang, Q. Tay, K. Zhang, Z. Chen, B. P. Binks, *Part. Part. Syst. Charact.* **2015**, *32*, 355–363.
[43] Y. Zhao, Y. Liu, Y. Wang, S. Li, Y. Liu, Z. L. Wang, P. Jiang, *Nano Energy* **2023**, *112*, 108464.
[44] Y. Nosaka, A. Y. Nosaka, *Chem. Rev.* **2017**, *117*, 11302–11336.
[45] A. Saiz-Lopez, J. M. C. Plane, A. R. Baker, L. J. Carpenter, R. von Glasow, J. C. Gómez Martín, G. McFiggans, R. W. Saunders, *Chem. Rev.* **2012**, *112*, 1773–1804.
[46] H. Huang, Y. Fan, Y. Wang, L. Wang, Y. Jiang, Y. Cheng, J. Wang, Y. Zhu, Y. Yang, *Matter* **2025**, *8*, 102154.

[47] Y. Ma, J. Pan, H. Rong, Y. Zhang, L. Liu, Y. Guo, J. Ai, Y. Yuan, N. Wang, *Adv. Sci.* **2025**, *12*, 2500993.
[48] W. Qu, Y. Yuan, C. Wen, J. Zhu, X. Liang, S. Chen, Z. Li, G. Cao, M. Zhang, *Energy Stor. Mater.* **2025**, *75*, 103993.
[49] Y. Li, H. Jia, Y. Hao, U. Ali, B. Liu, L. Zhang, L. Li, R. Lian, C. Wang, *Adv. Funct. Mater.* **2025**, *35*, 2419821.
[50] J. G. Calvert, S. E. Lindberg, *Atmos. Environ.* **2004**, *38*, 5105–5116.
[51] M. E. Goodsite, J. M. C. Plane, H. Skov, *Environ. Sci. Technol.* **2004**, *38*, 1772–1776.
[52] W. R. Simpson, R. von Glasow, K. Riedel, P. Anderson, P. Ariya, J. Bottenheim, J. Burrows, L. J. Carpenter, U. Frieß, M. E. Goodsite, D. Heard, M. Hutterli, H. W. Jacobi, L. Kaleschke, B. Neff, J. Plane, U. Platt, A. Richter, H. Roscoe, R. Sander, P. Shepson, J. Sodeau, A. Steffen, T. Wagner, E. Wolff, *Atmos. Chem. Phys.* **2007**, *7*, 4375–4418.
[53] Y. Zhao, Y. Wang, W. Xue, R. Cheng, X. Zheng, G. Zhu, D. Hu, H. Huang, C. Hu, D. Liu, *Adv. Mater.* **2024**, *36*, 2403097.
[54] D. Xing, X. Yuan, C. Liang, T. Jin, S. Zhang, X. Zhang, *Chem. Commun.* **2022**, *58*, 12447–12450.
[55] A. R. W. Raso, K. D. Custard, N. W. May, D. Tanner, M. K. Newburn, L. Walker, R. J. Moore, L. G. Huey, L. Alexander, P. B. Shepson, K. A. Pratt, *Proc. Natl. Acad. Sci. USA* **2017**, *114*, 10053–10058.
[56] Y. Guo, K. Li, S. Perrier, T. An, D. J. Donaldson, C. George, *Environ. Sci. Technol.* **2023**, *57*, 15580–15587.

Manuscript received: August 04, 2025
Revised manuscript received: September 02, 2025
Manuscript accepted: September 12, 2025
Version of record online: September 18, 2025